Available online at www.sciencedirect.com
ScienceDirect
International Journal of Heat and Mass Transfer 51 (2008) 4184–4194
International Journal of HEAT and MASS TRANSFER
www.elsevier.com/locate/ijhmt

On the inverse heat convection problem of the flow over a cascade of rectangular blades

Wen-Lih Chen *, Yu-Ching Yang

Clean Energy Center, Department of Mechanical Engineering, Kun Shan University, Yung-Kang City, Tainan 710-03, Taiwan, ROC

Received 11 September 2007; received in revised form 1 February 2008
Available online 26 March 2008

Abstract

In this study, an inverse algorithm based on the conjugate gradient method is applied to a steady flow over a cascade of rectangular blades to estimate the inlet flow temperature. The objective is to study the difficulties associated with inverse heat convection problems. Therefore, the measurement quantity has been deliberately placed at five different locations over the domain, each of them covered by a unique flow feature. The computation shows that at very low Reynolds number, the accuracy of the inverse method is not affected by the relative position between the estimated and measurement quantities. At a higher Reynolds number, however, the accuracy of the inverse method strongly depends on the relative position between the two quantities. The inverse method only returns satisfactory estimation for some cases but not others.

Keywords: Conjugate gradient inverse method; Heat convection; Cascade blades

1. Introduction

In recent years, inverse methods have been successfully applied to many heat conduction problems despite they are said to be ill-posed, and the studies of inverse heat conduction problem (IHCP) have offered alternatives, which can largely scale down sophisticated experimental work, to obtain accurate thermal quantities such as heat sources, material's thermal properties, and boundary temperature or heat flux distributions, in many heat conduction problems [1–5]. While there have been many reports on IHCP, there were relatively fewer studies on inverse heat convection problems [6–11]. Among them, many studies concerned flows over simple geometries such as pipe or channel flows where there is no complicated flow features like thicken boundary layers or flow separation, and there exist strong functional dependence of the measurement quantities on the estimated quantities [8–10]. There were only few studies dealing with more complicated flows such as the flow over multiple cylinders, 3D complex duct flow, or natural convection inside a cavity [6,7,11]. In these studies, however, the locations of the estimated and measurement quantities were so arranged, for example, very closed to heat flux boundary, that they are actually strongly affected by heat conduction rather than by heat convection [7,11]. Or, in the case of natural convection inside a cavity [6], the magnitude of heat source, which drives the entire cavity flow, at some points of the domain is estimated. In this instance, the measurement quantity is strongly dependent on the magnitude of heat source, thus prompting the success of an inverse solution. To the authors' best knowledge, there seems to be no successfully application of inverse method on a heat convection problem involving some flow features which result in a weak functional dependence of the measurement quantity on the estimated quantity, and there is no paper in open literature dedicated to address the difficulties facing inverse heat convection problems except for some simple statement like "due to their mathematical complexity as compared with the inverse heat conduction problems" [6].

* Corresponding author. Tel.: +886 62050496; fax: +886 62050509.
E-mail address: wlchen@mail.ksu.edu.tw (W.-L. Chen).

0017-9310/$ - see front matter © 2008 Published by Elsevier Ltd.
doi:10.1016/j.ijheatmasstransfer.2008.02.002

Nomenclature

C	blade's chord length (m)
H	blade's pitch length (m)
J	functional
J'	gradient of functional
k	thermal conductivity (W/m K)
L	length of the computational domain (m)
M	total number of measuring positions
P	dimensionless pressure
p	pressure (N/m^2)
Pr	Prandtl number, $Pr = \nu/\alpha$
q	direction of descent
Re	Reynolds number, $Re = V_0 C/\nu$
T_h	maximum temperature (K)
T_l	minimum temperature (K)
T^*	dimensionless temperature
u, v	velocity components in x and y coordinates (m/s)
U, V	dimensionless fluid velocity components
V_0	magnitude of inlet flow velocity (m/s)
X, Y	dimensionless coordinate
x_1, x_2	length parameters
y_1, y_2	length parameters
Δ	small variation quality
α	fluid's thermal diffusivity (m^2/s)
β	step size
γ	conjugate coefficient
η	very small value
Θ^*	dimensionless measured temperature
θ	angle of attack
λ	variable used in adjoint problem
ν	kinematic viscosity (m^2/s)
ρ	fluid density (kg/m^3)
σ	standard deviation

Superscripts

K	iterative number

Subscripts

f	fluid
s	solid

The success of the application of an inverse method essentially depends on strong functional relationship between the estimated and measurement quantities. In problems where the functional relation between the two quantities is weak, that is, a disturbance on the estimated quantity hardly affects the value of measurement quantity; an inverse solution is likely to fail. The governing equations for steady heat conduction problems are normally elliptic differential equations. The propagation of quantity in their solutions is not directional, that is, a disturbance at any point in the solution domain can reach all other points of the domain, regardless where they are located. In other words, all points in the solution domain, including boundaries, are strongly dependent on each others. Hence, the relative positions between estimated and measurement quantities in the solution domain is not an important issue regarding the success of an inverse solution. The governing equations for steady heat convection problems, on the other hand, are parabolic differential equations. The propagation of quantities in their solutions is intrinsically directional, that is, it is marching along the direction of stream. Consequently, an upstream quantity strongly affects its downstream quantity, whereas the downstream quantity has little effect on its upstream quantity. Under this circumstance, the relative position of estimated and measurement quantities become crucial to the success of an inverse solution. Essentially, the measurement quantity needs to be located downstream the estimated quantity for an inverse solution to be successful, for example, the case reported in [9]. (In fact, the governing equations for unsteady heat-conduction problems are also parabolic differential equations, and the same problem might become a major concern. However, transient heat-conduction problems are not in the scope of this paper, thus the issue is left to be addressed in some future paper.)

Although the issue aroused by directional propagation could be a major concern for inverse heat convection problems, the difficulty associated with them does not just end there. When the property of directional propagation combined with some complicated flow features creates yet another problem which might even sever the functional link between an upstream estimated quantity and a downstream measurement quantity. For instance, a quantity laid well inside a thick boundary or a separation bubble is unlikely to be strongly influenced by another quantity outside the boundary layer or separation bubble even the latter is located upstream the former. Therefore, a measurement quantity located in boundary layer region might only depend weakly, through diffusion rather than convection, on an estimated quantity in free-stream region. This might render the iterative regularization process of an inverse method futile, and an inverse solution might be failed largely due to this blockage on information transmission.

To further understand the above difficulties facing the inverse heat convection problems, we design a test case, which contains some complicated flow features, to be solved by an inverse method, in this case the conjugate gradient method (CGM) which transforms energy equation into an adjoint and a sensitivity equation and solves these three equations iteratively to minimize the estimation error [2,12–18], under various flow conditions. The test case chosen is the flow over a cascade of rectangular blades, pertinent to turbomachine aerodynamics. Although there is

no geometrical difference between the upper and lower sides of a rectangular blade, a non-zero angle of attack between the inlet flow and the blade would result in distinct flow features on both sides of the blade. On the pressure side (lower side), there is an attached boundary layer developing, while on the suction side (upper side), boundary layer could separate, forming a large separation bubble, under a high Reynolds number condition. The estimated quantity is the inlet temperature. The measurement quantity, on the other hand, is also temperature but is, respectively, located in five different downstream regions, each of them covered by some distinct flow features to allow the effects of these flow features on the accuracy of the inverse method to be examined.

2. Analysis

2.1. Direct problem

To illustrate the methodology for developing expressions for use in determining the unknown space-varying inlet temperature, we consider the following steady heat transfer problem.

Fig. 1 shows the geometry of the computational domain which surrounds the rectangular blade and extends, in the cross-stream direction, from the middle of one passage to the middle of the adjacent one. The domain also extends to a distance, in this case 0.3 chord lengths upstream and 2 chord lengths downstream the blade. The angle of attack for the inlet flow is θ, and the profile of inlet temperature distributions is $T_{\text{in}}(y)$. To simulate the effect of cooling fluid inside the blade, an imaginary boundary of zero thickness is placed at the center of the rectangular blade where minimum temperature T_{l} is maintained. On the surface of the blade, non-slip condition is assumed for the momentum equations. In terms of energy equation, however, the surface is actually a solid/fluid interface, and conjugate heat transfer takes place there. In current study, all physical properties of the solid and fluid materials are assumed to be constant, and gravity and buoyancy are not considered for simplicity. Therefore, this is a forced-convection heat transfer problem. To this end, the steady two-dimensional governing equations and boundary conditions for the test case can be written as *Navier–Stokes equations:*

$$\frac{\partial u}{\partial x}+\frac{\partial v}{\partial y}=0, \tag{1}$$

$$u\frac{\partial u}{\partial x}+v\frac{\partial u}{\partial y}=-\frac{\partial p}{\partial x}+\nu\left(\frac{\partial^2 u}{\partial x^2}+\frac{\partial^2 u}{\partial y^2}\right), \tag{2}$$

$$u\frac{\partial v}{\partial x}+v\frac{\partial v}{\partial y}=-\frac{\partial p}{\partial y}+\nu\left(\frac{\partial^2 v}{\partial x^2}+\frac{\partial^2 v}{\partial y^2}\right). \tag{3}$$

Energy equation:
For fluid:

$$u\frac{\partial T_{\text{f}}}{\partial x}+v\frac{\partial T_{\text{f}}}{\partial y}=\alpha\left(\frac{\partial^2 T_{\text{f}}}{\partial x^2}+\frac{\partial^2 T_{\text{f}}}{\partial y^2}\right), \tag{4}$$

For solid:

$$\frac{\partial^2 T_{\text{s}}}{\partial x^2}+\frac{\partial^2 T_{\text{s}}}{\partial y^2}=0. \tag{5}$$

Boundary conditions:
Inlet:

$$u=V_0\cos\theta,\quad v=V_0\sin\theta,\quad T=T_{\text{in}}(y), \tag{6}$$

Outlet:

$$\frac{\partial\phi}{\partial x}=0;\quad \phi=u,v,T, \tag{7}$$

Periodical boundaries:

$$\phi(x,0)=\phi(x,H);\quad \phi=u,v,T, \tag{8}$$

Solid/fluid interface:

$$u=v=0, T_{\text{f}}=T_{\text{s}},\quad \text{and}\quad k_{\text{f}}\frac{\partial T_{\text{f}}}{\partial n}=k_{\text{s}}\frac{\partial T_{\text{s}}}{\partial n}, \tag{9}$$

where n is the direction normal to the surface. Finally, for the imaginary boundary inside the solid blade:
Blade center:

$$T_{\text{s}}=T_{\text{l}}. \tag{10}$$

By introducing the following dimensionless parameters,

$$X=x/C,\quad Y=y/C,\quad U=u/V_0,\quad V=v/V_0,$$
$$P=\frac{p}{\frac{1}{2}\rho V_0^2},\quad T^*=T/(T_h-T_{\text{l}}), \tag{11}$$

where T_{h} and T_{l} are the maximum and minimum temperatures, respectively, Eqs. (1)–(10) become:

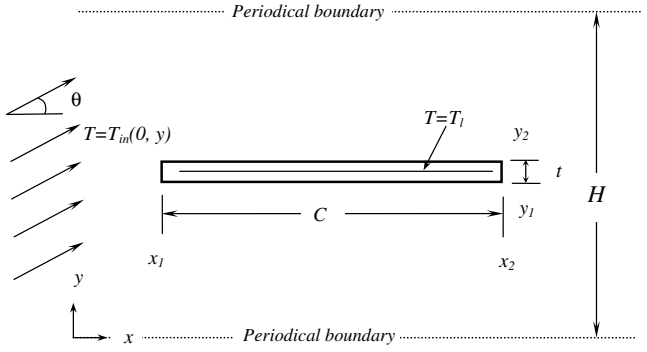

Fig. 1. Schematic of the blade configuration.

$$\frac{\partial U}{\partial X}+\frac{\partial V}{\partial Y}=0, \tag{12}$$

$$U\frac{\partial U}{\partial X}+V\frac{\partial U}{\partial Y}=-\frac{\partial P}{\partial X}+\frac{1}{Re}\left(\frac{\partial^2 U}{\partial X^2}+\frac{\partial^2 U}{\partial Y^2}\right), \tag{13}$$

$$U\frac{\partial V}{\partial X}+V\frac{\partial V}{\partial Y}=-\frac{\partial P}{\partial Y}+\frac{1}{Re}\left(\frac{\partial^2 V}{\partial X^2}+\frac{\partial^2 V}{\partial Y^2}\right), \tag{14}$$

$$U\frac{\partial T_{\mathrm{f}}^*}{\partial X}+V\frac{\partial T_{\mathrm{f}}^*}{\partial Y}=\frac{1}{Pr\cdot Re}\left(\frac{\partial^2 T_{\mathrm{f}}^*}{\partial X^2}+\frac{\partial^2 T_{\mathrm{f}}^*}{\partial Y^2}\right), \tag{15}$$

$$\frac{\partial^2 T_{\mathrm{s}}^*}{\partial X^2}+\frac{\partial^2 T_{\mathrm{s}}^*}{\partial Y^2}=0, \tag{16}$$

$$U=\cos\theta,\quad V=\sin\theta,$$
$$\text{and}\quad T_{\mathrm{f}}^*(0,Y)=T_{\mathrm{in}}^*(Y),\ \text{at } X=0, \tag{17}$$

$$\frac{\partial U}{\partial X}=\frac{\partial V}{\partial X}=0,\quad \frac{\partial T_{\mathrm{f}}^*}{\partial X}=0,\ \text{at } X=L/C, \tag{18}$$

$$U(X,0)=U(X,H/C),\quad V(X,0)=V(X,H/C),$$
$$T_{\mathrm{f}}^*(X,0)=T_{\mathrm{f}}^*(X,H/C), \tag{19}$$

$$U=V=0,\quad T_{\mathrm{f}}^*=T_{\mathrm{s}}^*,\ \text{and } k_{\mathrm{f}}\frac{\partial T_{\mathrm{f}}^*}{\partial X}=k_{\mathrm{s}}\frac{\partial T_{\mathrm{s}}^*}{\partial X},$$
$$\text{at } X=x_1/C \text{ and } X=x_2/C, \tag{20}$$

$$U=V=0,\quad T_{\mathrm{f}}^*=T_{\mathrm{s}}^*,\ \text{and } k_{\mathrm{f}}\frac{\partial T_{\mathrm{f}}^*}{\partial Y}=k_{\mathrm{s}}\frac{\partial T_{\mathrm{s}}^*}{\partial Y},$$
$$\text{at } Y=y_1/C \text{ and } Y=y_2/C, \tag{21}$$

where Re and Pr are Reynolds number and Prandtl number, and the subscripts f and s refer to the regions of fluid and solid, respectively. Since the velocity field is assumed not to be affected by temperature variation in a forced-convection problem, Eqs. (12)–(14) are solved independently prior to the inverse calculation. In terms of the inverse calculation, the direct problem only involves the energy Eqs. (15) and (16) and their boundary conditions. Here, the direct problem is concerned with the determination of the medium temperature when the space-varying inlet temperature $T_{\mathrm{in}}^*(Y)$, thermal properties, and boundary conditions are known.

2.2. Inverse problem

For the inverse problem, the space-varying inlet temperature $T_{\mathrm{in}}^*(Y)$ is regarded as being unknown, while everything else in Eqs. (15)–(21) is known. In addition, temperature readings at measurement locations are considered available. The objective of the inverse analysis is to predict the unknown space-varying inlet temperature $T_{\mathrm{in}}^*(Y)$ from knowledge of these temperature readings. Let the measured temperature at the measurement positions be denoted by $\Theta^*(X, Y)$. Then this inverse problem can be stated as follows: by utilizing the above mentioned measured temperature data $\Theta^*(X, Y)$, the unknown $T_{\mathrm{in}}^*(Y)$ is to be estimated over the specified domain.

The solution of the present inverse problem is to be obtained in such a way that the following functional is minimized:

$$J[T_{\mathrm{in}}^*(Y)]=\sum_{i=1}^{M}[T_{\mathrm{f}}^*(X_i,Y_i)-\Theta^*(X_i,Y_i)]^2, \tag{22}$$

here the subscript i refers to the ith temperature measuring position, M is the total number of measuring positions, and $T_{\mathrm{f}}^*(X_i, Y_i)$ is the estimated (or computed) temperature at the measurement location $(X, Y) = (X_i, Y_i)$. These quantities are determined from the solution of the direct problem given previously by using an estimated $\tilde{T}_{\mathrm{in}}^{*K}(Y)$ for the exact $T_{\mathrm{in}}^*(Y)$. Here $\tilde{T}_{\mathrm{in}}^{*K}(Y)$ denotes the estimated quantities at the Kth iteration.

2.3. Conjugate gradient method for minimization

The following iteration process based on the conjugate gradient method is now used for the estimation of $T_{\mathrm{in}}^*(Y)$ by minimizing the above functional $J[T_{\mathrm{in}}^*(Y)]$

$$\tilde{T}_{\mathrm{in}}^{*K+1}(Y)=\tilde{T}_{\mathrm{in}}^{*K}(Y)-\beta^K q^K(Y), K=0,1,2,\ldots, \tag{23}$$

where β^K is the search step size in going from iteration K to iteration $K+1$, and q^K is the direction of descent (i.e., search direction) given by

$$q^K(Y)=J'^K(Y)+\gamma^K q^{K-1}(Y), \tag{24}$$

which is conjugation of the gradient direction $J'^K(Y)$ at iteration K and the direction of descent $q^{K-1}(Y)$ at iteration $K-1$. The conjugate coefficient γ^K is determined from

$$\gamma^K=\frac{\int_{Y=0}^{H/C}[J'^K(Y)]^2\mathrm{d}Y}{\int_{Y=0}^{H/C}[J'^{K-1}(Y)]^2\mathrm{d}Y}\ \text{with } \gamma^0=0. \tag{25}$$

The convergence of the above iterative procedure in minimizing the functional J is proved in [2]. To perform the iterations according to Eq. (23), we need to compute the step size β^K and the gradient of the functional $J'^K(Y)$. In order to develop expressions for the determination of these two quantities, a "sensitivity problem" and an "adjoint problem" are constructed as described below.

3. Sensitivity problem and search step size

The sensitivity problem is obtained from the original direct problem defined by Eqs. (15)–(21) in the following manner. It is assumed that when $T_{\mathrm{in}}^*(Y)$ undergoes a variation $\Delta T_{\mathrm{in}}^*(Y)$, $T_{\mathrm{f}}^*(X,Y)$ and $T_{\mathrm{s}}^*(X,Y)$ are perturbed by $\Delta T_{\mathrm{f}}^*(X,Y)$ and $\Delta T_{\mathrm{s}}^*(X,Y)$, respectively. Then replacing in the direct problem T_{in}^* by $T_{\mathrm{in}}^*+\Delta T_{\mathrm{in}}^*$, T_{f}^* and T_{s}^* by $T_{\mathrm{f}}^*+\Delta T_{\mathrm{f}}^*$ and $T_{\mathrm{s}}^*+\Delta T_{\mathrm{s}}^*$, subtracting from the resulting expressions the direct problem, and neglecting the second-order terms, the following sensitivity problem for the sensitivity functions ΔT_{f}^* and ΔT_{s}^* can be obtained:

$$\frac{1}{Pr\cdot Re}\left(\frac{\partial^2\Delta T_{\mathrm{f}}^*}{\partial X^2}+\frac{\partial^2\Delta T_{\mathrm{f}}^*}{\partial Y^2}\right)=U\frac{\partial\Delta T_{\mathrm{f}}^*}{\partial X}+V\frac{\partial\Delta T_{\mathrm{f}}^*}{\partial Y}, \tag{26}$$

$$\frac{\partial^2\Delta T_{\mathrm{s}}^*}{\partial X^2}+\frac{\partial^2\Delta T_{\mathrm{s}}^*}{\partial Y^2}=0, \tag{27}$$

$$\Delta T_{\mathrm{f}}^*(0,Y)=\Delta T_{\mathrm{in}}^*(Y),\ \text{at } X=0, \tag{28}$$

$$\frac{\partial \Delta T_{\mathrm{f}}^*}{\partial x}=0,\ \text{at } x=L/C, \tag{29}$$

$$\Delta T_{\mathrm{f}}^*(X,0)=\Delta T_{\mathrm{f}}^*(X,H/C), \tag{30}$$

$$\Delta T_{\mathrm{f}}^*=\Delta T_{\mathrm{s}}^* \text{ and } k_{\mathrm{f}}\frac{\partial \Delta T_{\mathrm{f}}^*}{\partial X}=k_{\mathrm{s}}\frac{\partial \Delta T_{\mathrm{s}}^*}{\partial X},$$
$$\text{at } X=x_1/C \text{ and } X=x_2/C, \tag{31}$$

$$\Delta T_{\mathrm{f}}^*=\Delta T_{\mathrm{s}}^* \text{ and } k_{\mathrm{f}}\frac{\partial \Delta T_{\mathrm{f}}^*}{\partial Y}=k_{\mathrm{s}}\frac{\partial \Delta T_{\mathrm{s}}^*}{\partial Y},$$
$$\text{at } Y=y_1/C \text{ and } Y=y_2/C. \tag{32}$$

The sensitivity problem of Eqs. (26)–(32) can be solved by the same method as the direct problem.

The functional $J[\widetilde{T}_{\mathrm{in}}^{*K+1}(Y)]$ for iteration $K+1$ is obtained by rewriting Eq. (22) as

$$J[\widetilde{T}_{\mathrm{in}}^{*K+1}(Y)]=\int_{Y=0}^{H/C}\int_{X=0}^{L/C}\left[T_{\mathrm{f}}^*(\widetilde{T}_{\mathrm{in}}^{*K}-\beta^K q^K)-\Theta^*(X,Y)\right]^2 \cdot\delta(X-X_i)\cdot\delta(Y-Y_i)\mathrm{d}X\mathrm{d}Y, \tag{33}$$

where we replace $\widetilde{T}_{\mathrm{in}}^{*K+1}$ by the expression given by Eq. (23), and δ is the Dirac function which enforces the source term only appearing at (X_i, Y_i). If temperature $T_{\mathrm{f}}^*(\widetilde{T}_{\mathrm{in}}^{*K}-\beta^K q^K)$is linearized by a Taylor expansion, Eq. (33) takes the form

$$J[\widetilde{T}_{\mathrm{in}}^{*K+1}(Y)]=\int_{Y=0}^{H/C}\int_{X=0}^{L/C}[T_{\mathrm{f}}^*(\widetilde{T}_{\mathrm{in}}^{*K})-\beta^K\Delta T_{\mathrm{f}}^*(q^K)-\Theta^*(X,Y)]^2\cdot\delta(X-X_i)\cdot\delta(Y-Y_i)\mathrm{d}X\mathrm{d}Y \tag{34}$$

where $T_{\mathrm{f}}^*(\widetilde{T}_{\mathrm{in}}^{*K})$ is the solution of the direct problem at $(X, Y)=(X_i, Y_i)$ by using estimate $\widetilde{T}_{\mathrm{in}}^{*K}(Y)$ for exact $T_{\mathrm{in}}^*(Y)$. The sensitivity function $\Delta T_{\mathrm{f}}^*(q^K)$ is taken as the solution of Eqs. (26)–(32) at the measured position $(X, Y)=(X_i, Y_i)$ by letting $\Delta T_{\mathrm{in}}^*(Y)=q^K(Y)$ [13]. The search step size β^K is determined by minimizing the functional given by Eq. (34) with respect to β^K. The following expression results:

$$\beta^K=\frac{\int_{Y=0}^{H/C}\int_{X=0}^{L/C}\Delta T_{\mathrm{f}}^*(q^K)[T_{\mathrm{f}}^*(\widetilde{T}_{\mathrm{in}}^{*K})-\Theta^*]\cdot\delta(X-X_i)\cdot\delta(Y-Y_i)\mathrm{d}X\mathrm{d}Y}{\int_{Y=0}^{H/C}\int_{X=0}^{L/C}[\Delta T_{\mathrm{f}}^*(q^K)]^2\cdot\delta(X-X_i)\cdot\delta(Y-Y_i)\mathrm{d}X\mathrm{d}Y}. \tag{35}$$

3.1. Adjoint problem and gradient equation

To obtain the adjoint problem, Eqs. (15) and (16) are multiplied by the Lagrange multipliers (or adjoint functions) λ_{f}^* and λ_{s}^*, respectively, and the resulting expressions are integrated over the correspondent space domains. Then the result is added to the right hand side of Eq. (22) to yield the following expression for the functional $J[T_{\mathrm{in}}^*(Y)]$:

$$\begin{aligned}J[T_{\mathrm{in}}^*(Y)]=&\int_{Y=0}^{H/C}\int_{X=0}^{L/C}[T_{\mathrm{f}}^*(X,Y)-\Theta^*(X,Y)]^2\cdot\delta(X-X_i)\cdot\delta(Y-Y_i)\mathrm{d}X\mathrm{d}Y+\int_{Y=0}^{H/C}\int_{X=0}^{L/C}\lambda_{\mathrm{f}}^*(X,Y)\\&\cdot\left[\frac{1}{Pr\cdot Re}\left(\frac{\partial^2 T_{\mathrm{f}}^*}{\partial X^2}+\frac{\partial^2 T_{\mathrm{f}}^*}{\partial Y^2}\right)-U\frac{\partial T_{\mathrm{f}}^*}{\partial X}-V\frac{\partial T_{\mathrm{f}}^*}{\partial Y}\right]\mathrm{d}X\mathrm{d}Y\\&-\int_{Y=y_1/C}^{y_2/C}\int_{X=x_1/C}^{x_2/C}\lambda_{\mathrm{f}}^*(X,Y)\\&\cdot\left[\frac{1}{Pr\cdot Re}\left(\frac{\partial^2 T_{\mathrm{f}}^*}{\partial X^2}+\frac{\partial^2 T_{\mathrm{f}}^*}{\partial Y^2}\right)-U\frac{\partial T_{\mathrm{f}}^*}{\partial X}-V\frac{\partial T_{\mathrm{f}}^*}{\partial Y}\right]\mathrm{d}X\mathrm{d}Y\\&+\int_{Y=y_1/C}^{y_2/C}\int_{X=x_1}^{x_2/C}\lambda_{\mathrm{s}}^*(X,Y)\cdot\left(\frac{\partial^2 T_{\mathrm{s}}^*}{\partial X^2}+\frac{\partial^2 T_{\mathrm{s}}^*}{\partial Y^2}\right)\mathrm{d}X\mathrm{d}Y.\end{aligned} \tag{36}$$

The variation ΔJ is obtained by perturbing $T_{\mathrm{in}}^*(Y)$ by $\Delta T_{\mathrm{in}}^*(Y)$, $T_{\mathrm{f}}^*(X,Y)$ by $\Delta T_{\mathrm{f}}^*(X,Y)$, and $T_{\mathrm{s}}^*(X,Y)$ by $\Delta T_{\mathrm{s}}^*(X,Y)$ in Eq. (36), subtracting from the resulting expression the original Eq. (36) and neglecting the second-order terms. We thus find

$$\begin{aligned}\Delta J[T_{\mathrm{in}}^*(Y)]=&\int_{Y=0}^{H/C}\int_{X=0}^{L/C}2[T_{\mathrm{f}}^*(X,Y)-\Theta^*(X,Y)]\Delta T_{\mathrm{f}}^*\cdot\delta(X-X_i)\cdot\delta(Y-Y_i)\mathrm{d}X\mathrm{d}Y\\&+\int_{Y=0}^{H/C}\int_{X=0}^{L/C}\lambda_{\mathrm{f}}^*(X,Y)\cdot\left[\frac{1}{Pr\cdot Re}\left(\frac{\partial^2\Delta T_{\mathrm{f}}^*}{\partial X^2}+\frac{\partial^2\Delta T_{\mathrm{f}}^*}{\partial Y^2}\right)-U\frac{\partial\Delta T_{\mathrm{f}}^*}{\partial X}-V\frac{\partial\Delta T_{\mathrm{f}}^*}{\partial Y}\right]\mathrm{d}X\mathrm{d}Y\\&-\int_{Y=y_1/C}^{y_2/C}\int_{X=x_1/C}^{x_2/C}\lambda_{\mathrm{f}}^*(X,Y)\cdot\left[\frac{1}{Pr\cdot Re}\left(\frac{\partial^2\Delta T_{\mathrm{f}}^*}{\partial X^2}+\frac{\partial^2\Delta T_{\mathrm{f}}^*}{\partial Y^2}\right)-U\frac{\partial\Delta T_{\mathrm{f}}^*}{\partial X}-V\frac{\partial\Delta T_{\mathrm{f}}^*}{\partial Y}\right]\mathrm{d}X\mathrm{d}Y\\&+\int_{Y=y_1/C}^{y_2/C}\int_{X=x_1/C}^{x_2/C}\lambda_{\mathrm{s}}^*(X,Y)\cdot\left(\frac{\partial^2\Delta T_{\mathrm{s}}^*}{\partial X^2}+\frac{\partial^2\Delta T_{\mathrm{s}}^*}{\partial Y^2}\right)\mathrm{d}X\mathrm{d}Y,\end{aligned} \tag{37}$$

where δ is the Dirac function. Utilizing the boundary conditions of the sensitivity problem, we can integrate the second to the fourth double integral terms in Eq. (37) by parts. Then ΔJ is allowed to go to zero. The vanishing of the integrands containing ΔT_{f}^* and ΔT_{s}^* leads to the following adjoint problem for the determination of $\lambda_{\mathrm{f}}^*(X,Y)$ and $\lambda_{\mathrm{s}}^*(X,Y)$:

$$-U\frac{\partial\lambda_{\mathrm{f}}^*}{\partial X}-V\frac{\partial\lambda_{\mathrm{f}}^*}{\partial Y}=\frac{1}{Pr\cdot Re}\left(\frac{\partial^2\lambda_{\mathrm{f}}^*}{\partial X_2}+\frac{\partial^2\lambda_{\mathrm{f}}^*}{\partial Y_2}\right)+2[T_{\mathrm{f}}^*-\Theta^*]\cdot\delta(X-X_i)\cdot\delta(Y-Y_i), \tag{38}$$

$$\frac{\partial^2 \lambda_s^*}{\partial X^2} + \frac{\partial^2 \lambda_s^*}{\partial Y^2} = 0, \tag{39}$$

$$\lambda_f^* = 0, \quad \text{at} \quad X = 0, \tag{40}$$

$$\frac{1}{Pr \cdot Re} \frac{\partial \lambda_f^*}{\partial X} + U\lambda_f^* = 0, \quad \text{at} \quad X = L/C, \tag{41}$$

$$\lambda_f^*(X, 0) = \lambda_f^*(X, H/C), \tag{42}$$

$$\frac{k_s}{Pr \cdot Re}\lambda_f^* = k_f \lambda_s^* \quad \text{and} \quad \frac{1}{Pr \cdot Re}\frac{\partial \lambda_f^*}{\partial X} + U\lambda_f^* = \frac{\partial \lambda_s^*}{\partial X}, \quad \text{at} \quad X = x_1/C \quad \text{and} \quad X = x_2/C, \tag{43}$$

$$\frac{k_s}{Pr \cdot Re}\lambda_f^* = k_f \lambda_s^* \quad \text{and} \quad \frac{1}{Pr \cdot Re}\frac{\partial \lambda_f^*}{\partial Y} + V\lambda_f^* = \frac{\partial \lambda_s^*}{\partial Y}, \quad \text{at} \quad Y = y_1/C \quad \text{and} \quad Y = y_2/C. \tag{44}$$

One needs to note that in the case of measurement points located in the solid region, the source term $2[T_f^* - \Theta^*] \cdot \delta(X - X_i) \cdot \delta(Y - Y_i)$ will appear at the left hand side of Eq. (39) instead of in Eq. (38). Here, the adjoint problem is solved by the same method as the direct problem.

Finally the following integral term is left

$$\Delta J = \int_{Y=0}^{H/C} \left[\frac{1}{Pr \cdot Re}\frac{\partial \lambda_f^*(0, Y)}{\partial X} + U\lambda_f^*(0, Y)\right] \cdot \Delta T_{in}^*(Y) \mathrm{d}Y. \tag{45}$$

From the definition used in the reference [2], we have

$$\Delta J = \int_{Y=0}^{H/C} J'(Y) \cdot \Delta T_{in}^*(Y) \mathrm{d}Y, \tag{46}$$

where $J'(Y)$ is the gradient of the functional $J[T_{in}^*(Y)]$, a comparison of Eqs. (45) and (46) leads to the following form:

$$J'(Y) = \frac{1}{Pr \cdot Re}\frac{\partial \lambda_f^*(0, Y)}{\partial X} + U\lambda_f^*(0, Y). \tag{47}$$

3.2. Stopping criteria

If the problem contains no measurement errors, the traditional convergence condition for the minimization of the criterion is:

$$J(\widetilde{T}_{in}^{*K+1}) < \eta, \tag{48}$$

where η is a small specified number, can be used as the stopping criterion. However, the observed temperature information contains measurement errors; as a result, the inverse solution will tend to approach the perturbed input data, and the solution will exhibit oscillatory behavior as the number of iteration is increased [19]. Computational experience has shown that it is advisable to use the discrepancy principle [20] for determining the iteration process in the regular method. Assuming $T_f^* - \Theta^* \cong \sigma$, the stopping criteria η by the discrepancy principle can be obtained from Eq. (22) as

$$\eta = M\sigma^2, \tag{49}$$

where σ is the standard deviation of the measurement error. Then the stopping criterion is given by Eq. (48) with η determined from Eq. (49).

3.3. Computational procedure

The computational procedure for the solution of this inverse problem may be summarizes as follows:

Suppose $\widetilde{T}_{in}^{*K}(Y)$ is available at iteration K.

Step 1. Solve the direct problem given by Eqs. (15)–(21) for $T_f^*(X, Y)$ and $T_s^*(X, Y)$, respectively.
Step 2. Examine the stopping criterion given by Eq. (48) with η given by Eq. (49). Continue if not satisfied.
Step 3. Solve the adjoint problem given by Eqs. (38)–(44) for $\lambda_f^*(X, Y)$ and $\lambda_s^*(X, Y)$, respectively.
Step 4. Compute the gradient of the functional $J'(Y)$ from Eq. (47).
Step 5. Compute the conjugate coefficient γ^K and direction of decent $q^K(Y)$ from Eqs. (25) and (24), respectively.
Step 6. Set $\Delta T_{in}^*(Y) = q^K(Y)$ and solve the sensitivity problem given by Eqs. (26)–(32) for $\Delta T_f^*(X, Y)$ and $\Delta T_s^*(X, Y)$, respectively.
Step 7. Compute the search step size β^K from Eq. (35).
Step 8. Compute the new estimation for $\widetilde{T}_{in}^{*K+1}(y)$ from Eq. (23) and return to Step 1.

4. Results and discussion

It is intended, in this paper, to identify the difficulties facing inverse convection problem but not to study the flow over the rectangular blade. Therefore, only few flow conditions, which allow some distinct flow features near the blade to be developed, are investigated. In all, there are only three flow conditions where θ is fixed at 10 degree, and the Reynolds numbers are 1, 100, and 500, respectively. Also, the pitch of the blades is set to be equal to the chord length, while the thickness of the blade t is 1/20 of the chord length. The solid and fluid materials are assumed to be steel and air, with thermal conductivity of 43 W/mK and 0.024 W/mK, respectively. The numerical procedure in this paper is based on the unstructured-mesh, fully collocated, finite-volume code, 'USTREAM' developed by the corresponding author. This is the descendent of the structured-mesh, multi-block code of 'STREAM' [21]. The number of cells in the mesh used in this paper is 13,000.

In terms of the cascade flow, the boundary layer on the pressure side of the blade remains attached for all flow conditions; the boundary layer on the suction side, however, becomes separated at $Re = 500$ (see Fig. 3e). The estimated quantity is the temperature distribution at the inlet as mentioned earlier; the measurement quantity is also temperature but located at five different regions, respectively marked as positions 1–5 shown in Fig. 2, all over the domain. Here, positions 1 and 2 are both positioned vertically and

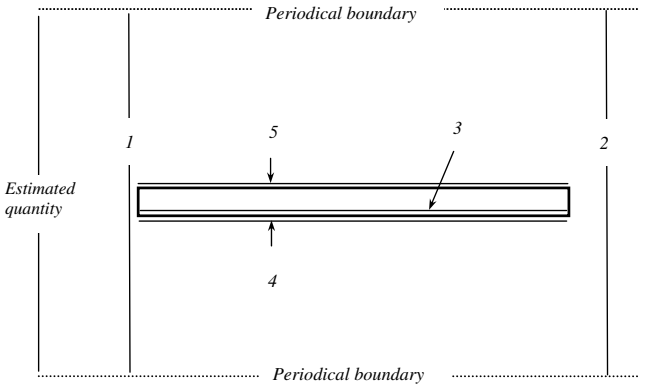

Fig. 2. Schematic of the five different measurement locations.

respectively, located upstream and downstream the blade. Position 3 is positioned horizontally and located inside the solid material near the pressure side of the blade. Position 4 is on the pressure side, and position 5 is on the suction side; both are positioned horizontally and inside blade's boundary layer. The purpose of the five measurement position arrangements is to create different relative positions with the estimated quantity. Among them, quantities at some of the measurement positions are strongly influenced by the convection of the upstream estimated quantity (like positions 1 and 2), but others are not (positions 3, 4, and 5). This allows the effects of convection on the accuracy of the inverse method to be investigated.

Fig. 3 shows the streamlines and temperature contours of the domain at the three different Reynolds numbers. The streamlines in Fig. 3a, c, and e, clearly show the flow patterns at the three different Reynolds numbers. From the temperature contours given in Fig. 3b, d, and f, on the other hand, it is evident that the distributions of temperature over the entire domain are highly dependent on Reynolds number. At low Reynolds number ($Re = 1$ in Fig. 3b), the effect of convection is weak, and low temperature from the blade is able to diffuse into a large portion of the domain, including some upstream region of the blade. However, as Reynolds number increases, higher temperature from the inlet has swept through the entire domain due to stronger convection, and lower temperature can only propagate to regions adjacent to and downstream of the blade but not to the upstream region of the blade (see Fig. 3d and f). These plots clearly demonstrate that convection becomes the predominant mean of quantity propagation at a high Reynolds number condition.

Comparing Eq. (15) with (38), the governing equations of the direct and the adjoint problems for the fluid domain, one can note that their convection terms are at different sign. This suggests that from the point of λ_f^*, the flow is totally at the reverse direction of the flow viewed in the direct problem. This is an important aspect for the regularization mechanism of the inverse method, and its importance is explained as follows: Eq. (38) implies that the magnitude of λ_f^* over the domain is mainly generated by the source term $2(T_f^* - \Theta^*)$ at the measurement location; in other words, λ_f^* is fed by the disagreement between the computed and measured temperatures at the measurement location. The amount of the disagreement needs to be transported back, through λ_f^*, to where the estimated quantity $\widetilde{T}_{in}^*$ is located, in this case, the inlet boundary, for $\widetilde{T}_{in}^*$ to be corrected by Eq. (24). The reversed flow in the adjoint problem happens to serve this purpose by transporting the information back to the upstream estimated-quantity location through convection. In a brief summary, the iterative regularization process works like this: an inaccurate upstream temperature profile $\widetilde{T}_{in}^*$ produces some disagreement $(T_f^* - \Theta^*)$ at the downstream measurement location. This disagreement generates λ_f^*, which is transported back to the inlet by the reversed flow and then corrects the estimated quantity $\widetilde{T}_{in}^*$. From this process, it is readily to realize that the success of the whole process largely depends on the information transmission forward and backward the estimated and measurement locations. In a complex flow like the current test case, the information transmission between two locations could be hampered by some flow features mentioned in the introduction section, and the accuracy of the inverse solution might deteriorate as a consequence. For the rest of this section, the results at the five different measurement locations will be presented, and the effects of flow convection on the accuracy of the inverse method will be discussed.

Since convection plays an important role in the current problem, we need to understand the directions of the convection of quantities, especially the convection of λ_f^*. A streakline plot, from the aspect of λ_f^*, with streaks originate from the measurement location will provide a clear picture of the convection of λ_f^* through the domain. In the following, only the streaklines for $Re = 100$ or 500 will be plotted but not for $Re = 1$. This is because at very low Reynolds number, conduction is predominant, and convection becomes less significant or even irrelevant to the accuracy of the inverse solutions. Fig. 4a shows the streaklines of the measurement location 1, while Fig. 4b shows the exact and the resulted estimation inlet temperature distributions at three different Reynolds numbers. Here, the exact inlet temperature distribution is assumed to be constant high temperature, that is $T_{in}^*(Y) = 1$, and all inverse calculations start from an initial guess of $\widetilde{T}_{in}^* = 0.5$. In Fig. 4a, it can be seen that streaks originated from location 1 almost cover the entire inlet boundary, signifying that λ_f^* generated at the measurement location can be effectively transported back to the inlet through convection. This largely contributes to the success of the inverse solutions as can be seen from Fig. 4b, where the maximum difference between the exact and estimated temperature for all Reynolds numbers is less than 2%. The streaklines and the results of the inverse calculation for measurement location 2 are given in Fig. 5. Here, the streaklines for $Re = 100$ and 500 are, respectively, depicted in Fig. 5a and b. Despite a portion of location 2 is inside the blade's wake, the streaks originate from this location still manage to pass around the blade and reach most of

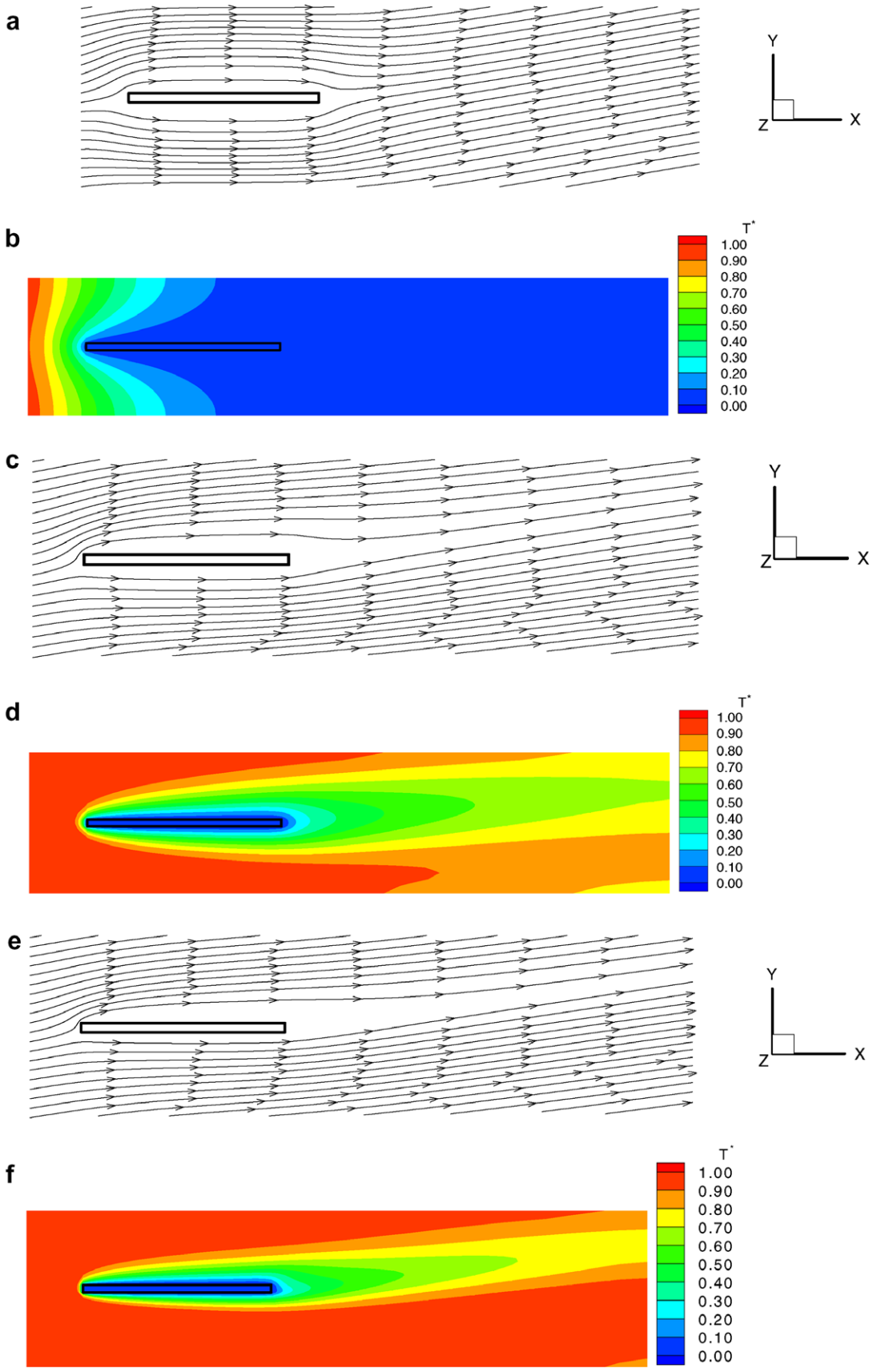

Fig. 3. Streamlines and Temperature contours over the computational domain at $\theta = 10°$ and three different Reynolds numbers; (a) streamlines at $Re = 1$, (b) temperature contours at $Re = 1$, (c) streamlines at $Re = 100$, (d) temperature contours at $Re = 100$, (e) streamlines at $Re = 500$, and (f) temperature contours at $Re = 500$.

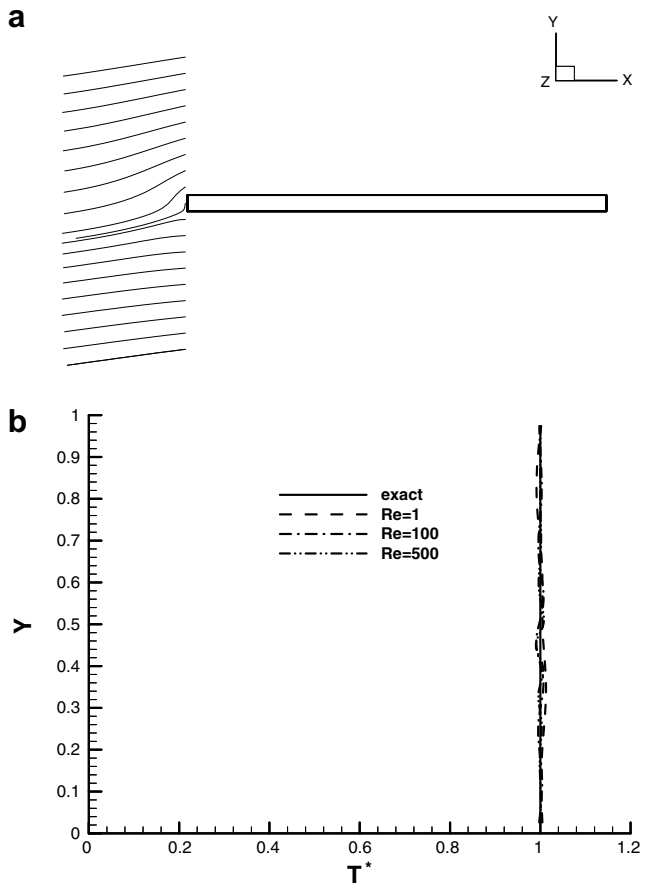

Fig. 4. Streakline originated from measurement location 1 and the estimated inlet temperature distributions at three different Reynolds numbers; (a) streakline at $Re = 500$ and (b) estimated temperature distributions.

the inlet boundary similar to the case of location 1. As a result, excellent agreement between the exact and estimated temperatures is returned as shown in Fig. 5c.

Measurement location 3 is a special one among the five because it is located inside the solid blade. If the inverse method performs well at this location, it would open a wide range of applications in turbomachine flows because the inlet flow temperature, which is difficult to measure [22], can be estimated with much ease by just measuring the temperature inside the solid blade. Also for location 3, there is no need to plot streaks originated from it. The λ_f^* generated at this location must be first transferred through diffusion to the adjacent fluid region and then through convection to the inlet boundary. The adjacent fluid region in this case is the region inside the pressure side boundary layer, thus the accuracy of the inverse solutions from this location should be similar to that of location 4 (will be discussed later). From another point, the results of this location can be regarded as the baseline solution for the case without direct convective transfer of λ_f^* from the measurement location to the estimated location. The estimated and exact temperatures for this location are given in Fig. 6. It can be seen that satisfactory accuracy is only maintained for

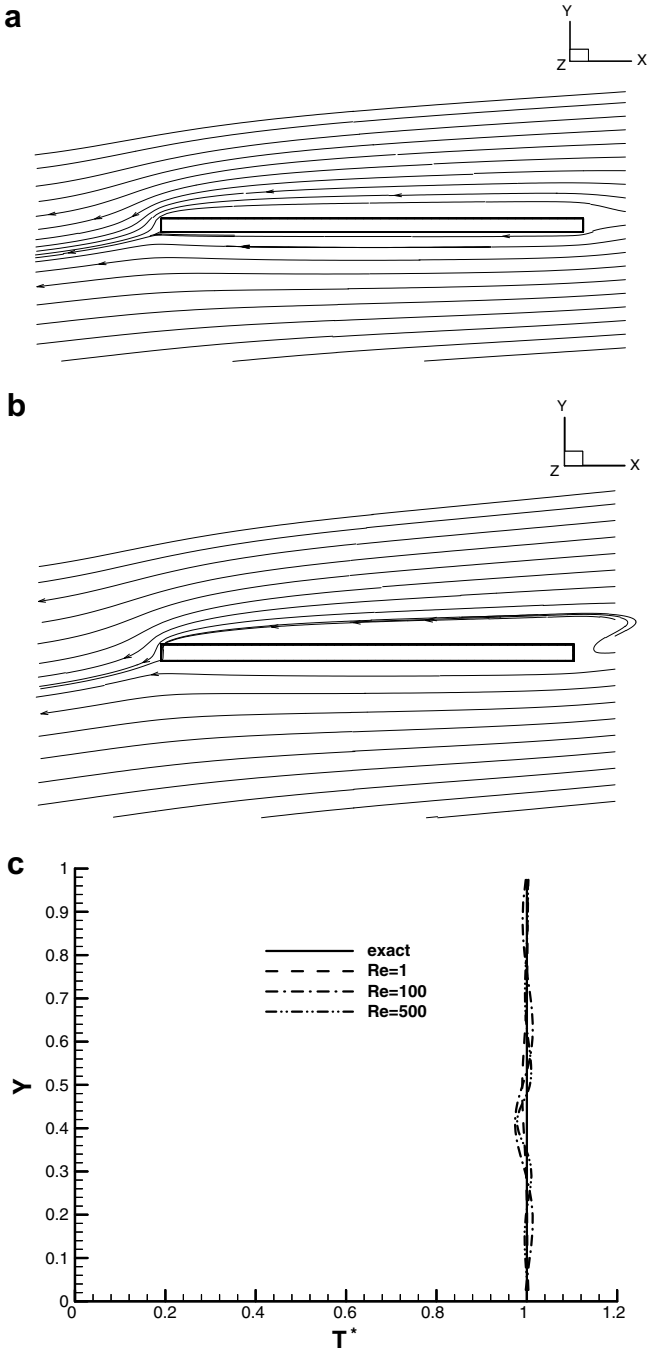

Fig. 5. Streakline originated from measurement location 2 and the estimated inlet temperature distributions at three different Reynolds numbers; (a) streakline at $Re = 100$, (b) streakline at $Re = 500$, and (c) estimated temperature distributions.

$Re = 1$, and accuracy deteriorates as the Reynolds number increases. Here, the maximum error for $Re = 500$ reaches 17%.

The results for locations 4 and 5 are shown in Figs. 7 and 8, respectively. Figs. 7a, 8a and b indicate that the streaks originated from both locations all concentrate to a very small part of the inlet boundary and leave the rest of the inlet uncovered. As a result, the inverse method only returns accuracy solutions for both locations at $Re = 1$,

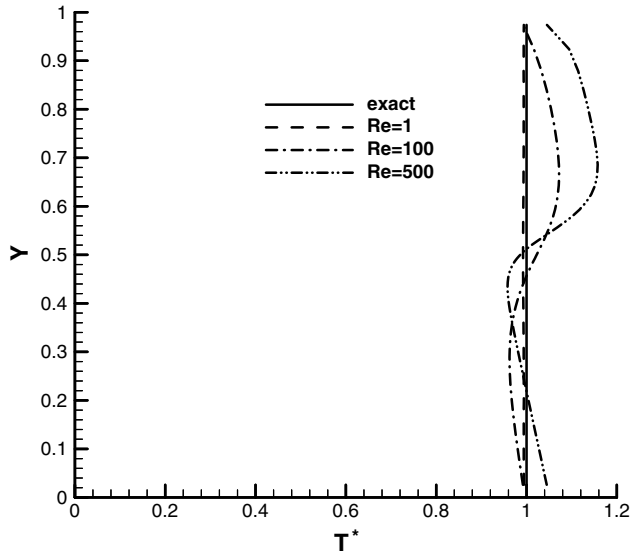

Fig. 6. The estimated inlet temperature distributions at three different Reynolds numbers of location 3.

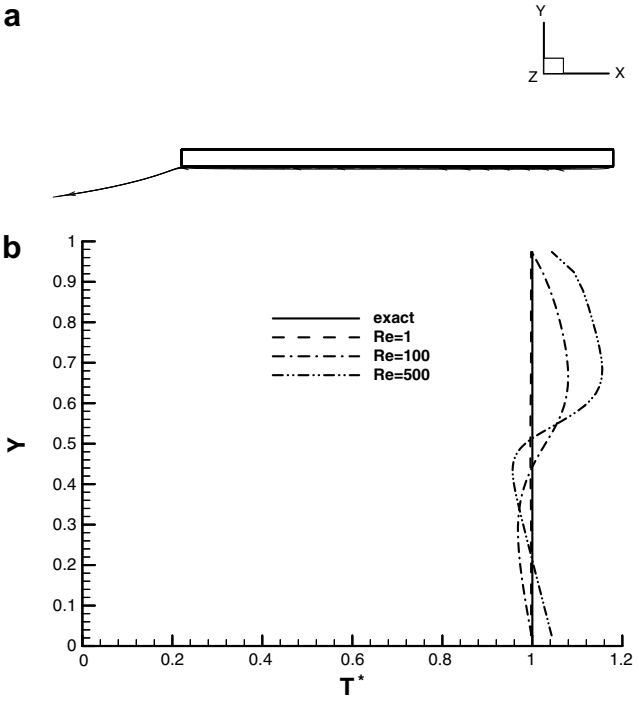

Fig. 7. Streakline originated from measurement location 4 and the estimated inlet temperature distributions at three different Reynolds numbers; (a) streakline at $Re = 500$ and (b) estimated temperature distributions.

and again the solution accuracy is worsening as Reynolds number increases just like the case of location 3. In the case of location 5, it is interesting to note that at $Re = 500$, only a small portion of the streaks reach the inlet boundary, and the rest are just circling inside the large separation region (Fig. 8b). Consequently, the case returns the largest error, at about 20% over-estimation, among all test cases in this

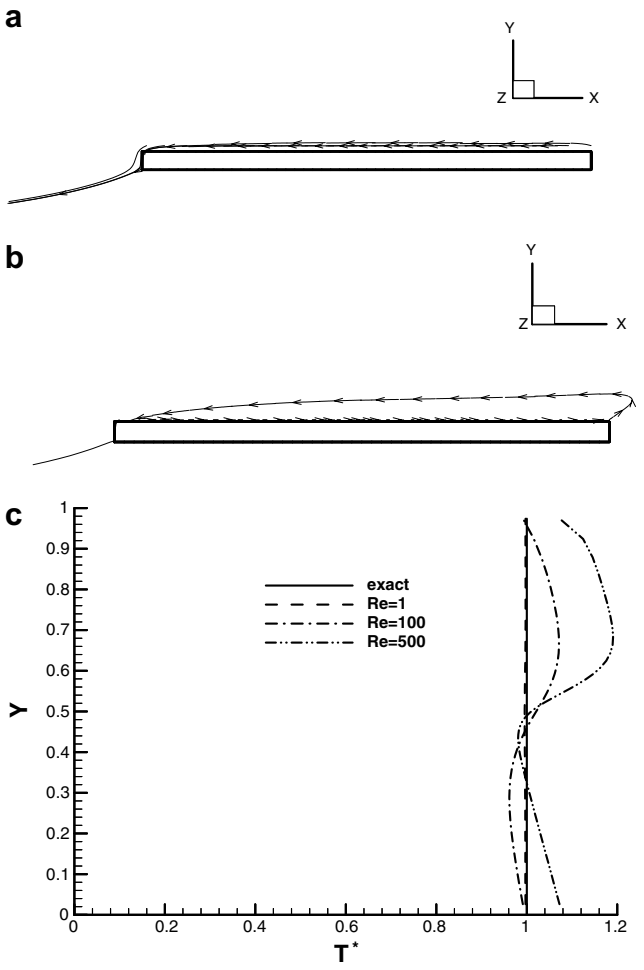

Fig. 8. Streakline originated from measurement location 5 and the estimated inlet temperature distributions at three different Reynolds numbers; (a) streakline at $Re = 100$, (b) streakline at $Re = 500$, and (c) estimated temperature distributions.

paper for the inlet temperature (see Fig. 8c). Comparing the estimated temperatures between locations 3 and 4 (Figs. 6 and 7b), it is not surprising to see that there are quite similar for all Reynolds numbers even though one is inside solid, and the other is in fluid. The reasons for this have been explained in the discussion of location 3.

5. Conclusion

A conjugate gradient inverse method has been applied to estimate the inlet temperature distribution for the flow over a cascade of rectangular blade pertinent to turbomachine aerodynamics. There exist some complex flow features in this flow at high Reynolds number conditions which allow the difficulties of applying the inverse method on heat convection problems to be manifested. The accuracy of the inverse method is highly dependent on the relative position between estimated and measurement quantities at higher Reynolds number. Several conclusions can be drawn from the current investigation as follows:

1. At very low Reynolds number, say $Re = 1$, the accuracy of the inverse method is insensitive to the relative positions between the estimated and measurement quantities, and the method returns very good results at all measurement locations. This is because heat conduction is predominant, and there exists strong functional dependence between estimated and measurement quantities regardless their relative positions.
2. At higher Reynolds numbers, $Re = 100$ or 500, convective heat transfer, which is marching streamwise, becomes more prominent than heat conduction. Strong functional dependence of the measurement quantities on the estimated quantity only exist for some relative positions but not others. In general, if the measurement quantity is located in the free stream region downstream the estimated quantity and lines up in parallel with the later, the inverse method performs well and returns accurate estimation. However, if the measurement quantity is situated inside the blade's boundary layer or in a separation region, the information transmission forward and backward the estimated and measurement quantities is limited. This seriously hampers the effectiveness of the iterative regularization process of the inverse calculation and results in the inverse method failing to produce any credible estimation for the inlet temperature.
3. Embedding measuring equipment inside the solid blade would give rise to more or less similar result to that of obtaining reading inside blade's boundary layer. This implies that it is not yet feasible, at the current stage, to apply the conjugate gradient inverse method to turbomachinery flows.

Acknowledgement

This work was supported by the National Science Council, Taiwan, Republic of China, under the Grant numbers NSC 95-2221-E-168-033 and NSC 96-2221-E-168-018.

References

[1] Y. Jarny, M.N. Ozisik, J.B. Bardon, A general optimization method using an adjoint equation for solving multidimensional inverse heat conduction, Int. J. Heat Mass Transfer 34 (1991) 2911–2919.
[2] O.M. Alifanov, Inverse Heat Transfer Problem, Springer-Verlag, Berlin, 1994.
[3] K. Kurpisz, A.J. Nowak, Inverse Thermal Problems, Computational Mechanics Publications, Southampton, 1995.
[4] H.M. Park, O.Y. Chung, J.H. Lee, On the solution of inverse heat transfer problem using the Karhunen-Loeve Galerkin method, Int. J. Heat Mass Transfer 42 (1999) 127–142.
[5] Y.C. Yang, S.S. Chu, W.J. Chang, Thermally-induced optical effects in optical fibers by inverse methodology, J. Appl. Phys. 95 (2004) 5159–5165.
[6] H.M. Park, O.Y. Chung, An inverse natural convection problem of estimating the strength of a heat source, Int. J. Heat Mass Transfer 42 (1999) 4259–4273.
[7] C.H. Huang, W.C. Chen, A three-dimensional inverse forced convection problem in estimating surface heat flux by conjugate gradient method, Int. J. Heat Mass Transfer 43 (2000) 3171–3181.
[8] M. Prud'homme, S. Jasmin, Determination of a heat source in porous medium with convective mass diffusion by an inverse method, Int. J. Heat Mass Transfer 46 (2003) 2065–2075.
[9] Y.K. Hong, S.W. Baek, Inverse analysis for estimating the unsteady inlet temperature distribution for two-phase laminar flow in a channel, Int. J. Heat Mass Transfer 49 (2006) 1137–1147.
[10] C.K. Chen, L.W. Wu, Y.T. Yang, Application of the inverse method to the estimation of heat flux and temperature on the external surface in laminar pipe flow, Appl. Thermal Eng. 26 (2006) 1714–1724.
[11] W.L. Chen, Y.C. Yang, An inverse problem in determining the heat transfer rate around two in line cylinders placed in a cross stream, Energy Convers. Manage. 48 (2007) 1996–2005.
[12] R.M. Hestenes, E. Stiefel, Methods of conjugate gradients for solving linear systems, J. Res. Natl. Bur. Stand. 49 (1952) 409–436.
[13] O.M. Alifanov, N.V. Kerov, Determination of external thermal load parameters by solving the two-dimensional inverse heat conduction problem, J. Eng. Phys. 41 (1981) 581–586.
[14] K.E. Atkinson, An Introduction to Numerical Analysis, second ed., John Wiley & Sons, 1989.
[15] W.J. Chang, T.H. Fang, C.I. Weng, Inverse determination of the cutting force on nanoscale processing using atomic force microscopy, Nanotechnology 15 (2004) 427–430.
[16] W.J. Chang, T.F. Fang, An inverse method for determining the interaction force between the probe and sample using scanning near-field optical microscopy, Phys. Lett. A 348 (2006) 260–265.
[17] Y.C. Yang, Simultaneously estimating the contact heat and mass transfer coefficients in a double-layer hollow cylinder with interface resistance, Appl. Thermal Eng. 27 (2007) 501–508.
[18] W.L. Chen, Y.C. Yang, H.L. Lee, Inverse problem in determining convection heat transfer coefficient of an annular fin, Energy Convers. Manage. 48 (2007) 1081–1088.
[19] V.S. Arpaci, P.S. Larsen, Convective Heat Transfer, Prentice-Hall, Englewood Cliffs, NJ, 1884.
[20] O.M. Alifanov, Application of the regularization principle to the formulation of approximate solution of inverse heat conduction problem, J. Eng. Phys. 23 (1972) 1566–1571.
[21] F.S. Lien, W.L. Chen, M.A. Leschziner, A multiblock implementation of a non-orthogonal, collocated finite volume algorithm for complex turbulent flows, Int. J. Numer. Methods Fluids 23 (1996) 567–588.
[22] Z. Mazur, A.H. Rossette, R.G. Illescas, A.L. Ramirez, Analysis of conjugate heat transfer of a gas turbine first stage nozzle, Appl. Thermal Eng. 26 (2006) 1796–1806.